PROCEEDINGS OF SPIE

SPIEDigitalLibrary.org/conference-proceedings-of-spie

Expanding the transmission window of visible-MWIR chalcogenide glasses by silicon nitride doping

Ellis Archer, Dichu Xu, Chris Craig, Katrina Morgan, Ioannis Zeimpekis

Ellis Archer, Dichu Xu, Chris Craig, Katrina Morgan, Ioannis Zeimpekis, "Expanding the transmission window of visible-MWIR chalcogenide glasses by silicon nitride doping," Proc. SPIE 12518, Window and Dome Technologies and Materials XVII
, 1251803 (13 June 2023); doi: 10.1117/12.2663345

SPIE.

Event: SPIE Defense + Commercial Sensing, 2023, Orlando, Florida, United States

Expanding the transmission window of visible-MWIR chalcogenide glasses by silicon nitride doping

Ellis Archer[a], Dichu Xu[a], Chris Craig[a], Katrina Morgan[a], Ioannis Zeimpekis[a]
[a]University of Southampton, Southampton, Hampshire SO17 1BJ.

ABSTRACT

Gallium Lanthanum sulphur-oxide (GLSO) glass is an excellent candidate for a window/dome material ought to its wideband transmission window from visible to MWIR. The suitable optical transmission from 0.45-8 microns is supplemented by its superior thermal and mechanical properties to contemporary materials, such as Cleartran™ zinc sulphide. In this work, the properties of GLSO were enhanced by doping with small concentrations of silicon nitride (≤ 0.5 M%), which expanded the transmission window to encompass all the visible spectra. Nano-indentation demonstrated that the hardness and elastic modulus slightly improved. Overall, the improvements demonstrated here make this glass an even better solution when compared to the state-of-the-art for use in single-optic windows and domes.

Keywords: Gallium, Lanthanum, Sulphide, Oxide, Visible, MWIR, Silicon, Nitride

1. INTRODUCTION

1.1 Optics for Electro-optical Infrared Devices

Currently, there is a huge development of electro-optical infrared (EO-IR) devices for various applications, including situational awareness, self-defense and surveillance in aerospace.[1–3] Overall, while advancements are being made, larger constraints in size and weight are required, especially with the prevalence of Unmanned Aerial Vehicle (UAV) technology. Generally, EO-IR devices have various optical lenses, each with the requirement to transmit a certain section of wavelengths. This includes visible (0.4-0.7 μm), NIR (0.7-1 μm), SWIR (1-2.5 μm), MWIR (3-5 μm) and LWIR (8-14 μm). To achieve the desired outcome of minimizing the size and weight of the EO-IR devices, one very desirable method is to have a widespan optical material that can transmit all the relevant wavelengths. For certain applications such as in aerospace, this material should also be resistant to harsh environments, such as solid/liquid erosion,[4,5] corrosion[6] and thermal shock[7].

There are numerous polycrystalline materials that have properties for this application. Aluminum oxynitride (ALON)[8] has full visible to MWIR transparency and has very high mechanical robustness, while lacking the transparency to LWIR. Multispectral Zinc Sulphide has visible to LWIR transparency, while lacking mechanical and thermal resistance.[9] There are also glassy materials that can transmit suitable wavelengths, which are generally chalcogenides.[10] Examples include, As_2Se_3 and $Ge_{33}As_{12}Se_{55}$, which have transmissions of 1-12 μm and 0.7-14 μm respectively. While these chalcogenide glasses are quicker to make and easier to manufacture into lenses, they tend to have poor mechanical and thermal properties.

1.2 Development New Materials for Optics

The Novel Glass Group at the Optoelectronics Research Center of the University of Southampton has been developing gallium lanthanum sulphide multispectral glasses for a long time.[11] The GLS glass has a very wide transparency (0.5-10 microns), while having much better thermal and mechanical properties than the other arsenic-based chalcogenide glasses, such as As_2Se_3. Due to it being a glassy material it can still be molded into complex shapes easily (figure 1) by heating above its molding temperature.[11] However, due to the non-volatile components, it can use a flowing argon melt instead of the sealed ampoule method used with other chalcogenide glasses that also incorporate toxic arsenic in their compositions. This method is easier and safer to upscale. GLS can also incorporate selenides and oxides to shift the transmission window

Window and Dome Technologies and Materials XVII, edited by W. Howard Poisl, Proc. of SPIE
Vol. 12518, 1251803 · © 2023 SPIE · 0277-786X · doi: 10.1117/12.2663345

based on specific requirements. The resulting GLSSe has a transmission of 0.55-12 microns, while the GLSO has a transparency from 0.45-8 microns.

A commonly used method to improve the optical, thermal and mechanical properties of glasses is to incorporate appropriate dopants.[12–14] This paper demonstrates a method of doping GLSO glass using silicon nitride to enhance its optical properties. The scope of this work has been to expand the glass transmission further in the visible and therefore GLSO was a good starting candidate because it transmits nearly all the visible, while incorporating the MWIR window. The aim has been a large enough transmission shift that results in an entirely clear glass that still transmits to MWIR. There are examples of EO-IR devices that utilize visible-MWIR exclusively.[15] So this material could provide an alternative that is easier to shape and quicker to manufacture than existing visible-MWIR materials, like ALON. To characterize the doped glasses, different concentrations of silicon nitride dopant were introduced in GLSO, with the optical and mechanical properties tested and compared to the GLSO without dopants.

Figure 1. Polished spheres made from GLS

2. METHOD AND MATERIALS

2.1 Glass Preparation

The $(65)Ga_2S_3$-$(35-x)La_2O_3$-$(x)Si_3N_4$ (GLSO) glass system samples, with x varying from 0.2-1, were fabricated using the flowing argon melting technique described by Hewak et al.[16] The samples were diamond cut into 1 mm thick samples and polished to optical quality on both faces.

2.2 Transmission Characterization

A UV-VIS (Cary-500) spectrometer was used to determine the optical transmission from 200-1500 nm. An FTIR (Cary-670) spectrometer was used to determine the transmission from 1.66-25 um.

2.3 Elemental Analysis

Elemental analysis was done using a Zeiss Leo 1450VP SEM with an Oxford Instruments X—act EDS (energy dispersive spectrometer) elemental analyzer with a 10mm window. The samples were sputtered with 20nm of gold and imaged at 15 mm working distance, with an electron high tension of 20 Kv. Two sections of the image were selected for elemental analysis, which was done on the software Aztec 5.0 SP1. An average and standard deviation was generated from the two sections of each sample.

2.4 Mechanical Characterization

Nanoindentation tests (NanoTest Vantage system, MicroMaterials Ltd., UK) were performed on undoped and doped glasses using a Berkovich diamond tip (Young ’s modulus Ei = 1141 GPa; Poisson’s ratio υi = 0.07) at room temperature.

Nanoindentation testing was conducted in a depth-control method, at loading and unloading rates of 10 mN/s, with a dwell of 15 s at peak load to allow for creep. For each specimen, indentations were run to varying maximum indentation depth, ranging from 100 nm to 1000 nm, with intervals of 20 nm (100~500 nm), 50 nm (500~700 nm) and 100 nm (700~1000 nm). To minimise the impact of surface roughness on measurements, targeted indentation depth was maintained at a minimum of 100 nm. Ten individual indentations were performed at each indentation depth, and the hardness and modulus values were averaged.

The nanoindentation hardness (H) and reduced modulus (Er) were calculated using the Oliver-Pharr.[17] The reduced modulus Er involves the Young's modulus and Poisson's ratio of the diamond indenter and the specimen, and can be expressed by equation 1 as follow:

$$\frac{1}{Er} = \frac{1 - Vi^2}{Ei} + \frac{1 - Vs^2}{Es}$$

Equation 1. Converting reduced modulus (Er) to Young's modulus (Ei) of substrate.

Where Es is Young's modulus of substrate, and Vs is Poisson's ratio of substrate. The Ei and Vi is the Young's modulus and Poisson's ratio of the diamond indenter. Due to the extremely high young's modulus of diamond, the Young's modulus is very close to the reduced modulus. Therefore, for the sake of simplicity, the reduced modulus was displayed in this paper.

3. RESULTS

3.1 Glass Formation and Elemental Composition

Following quenching, the compositions x=0.2-0.5 formed full glassy ingots, clear of any striations and bubbles. At x=0.6, there were obvious crystalline regions dispersed throughout the glassy matrix. At any higher concentrations, the entire ingot crystallized. This demonstrated that the silicon nitride could possibly be forming nucleation points for crystallization, and subsequently has a maximum tolerated concentration. The elemental analysis showed the increasing concentrations of silicon in the glass, though no nitrogen was detected in any of the compositions (table 1). The likely reason is due to EDS struggling to detect lighter elements that have such low concentrations. The oxygen levels of all the samples increased by about 10 M%, at the expense of some of the sulphur, gallium and lanthanum of each sample. This is expected in the melting setup used, which was unable to fully purge the oxygen from the furnace. Generally, this would affect the IR cutoff point of the final glass. However, since all the glasses underwent the same oxygen increase, it can be inferred that any transmission changes are due to the dopant.

Table 1. Elemental compositions of GLSO and the doped GLSO glasses, obtained with EDS.

Glass Composition (Si_3N_4 M%)	Ga	S	La	O	Si	N
0	21.79 ± 0.54	32.68 ± 0.65	13.98 ± 0.38	31.55 ± 1.58	0	0
0.2	23.18 ± 0.39	33.62 ± 1.1	12.44 ± 0.21	30.69 ± 1.27	0.08 ± 0.1	0
0.3	22.93 ± 0.06	32.22 ± 0.45	11.91 ± 0.55	32.86 ± 1.07	0.09 ± 0	0
0.4	22.89 ± 0.5	32.8 ± 0.06	12.16 ± 0.69	31.97 ± 0.14	0.19 ± 0.01	0
0.5	22.31 ± 0.29	33.92 ± 0.1	11.5 ± 0.09	32 ± 0.27	0.28 ± 0.01	0

3.2 Transmission Measurements

As shown in figure 2, after cutting and polishing the glasses from the produced raw ingots, it was clear to the naked eye through a comparison with the undoped glass that the 0.5 M% silicon nitride doped glass had a shift in the visible range. Following this, transmission measurements were taken of the samples from UV to LWIR. The UV-VIS spectra of figure 3 demonstrates that, with increasing concentrations of silicon nitride, the visible edge experiences a blue shift. The highest concentration of 0.5 % silicon nitride shifted the transmission by 50 nm, incorporating nearly all the visible spectrum. An interesting result is that the 0.3 M% shifted further than the 0.4 M%, though this could just be due to normal statistical

error resulting from the concentrations being so close to one another but also due to slight variations in the overall composition. However, the trend with increasing doping is clearly showing a blue shift when compared to the undoped sample. The FTIR results of figure 4 demonstrate that the glass with the highest concentration of silicon nitride still maintained its transparency to MWIR and past 5 microns.

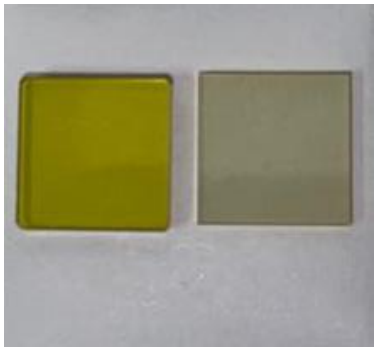

Figure 2. A photograph of an undoped GLSO sample (left) and a GLSO sample with the maximum tolerated 0.5 M% doping of silicon nitride (right).

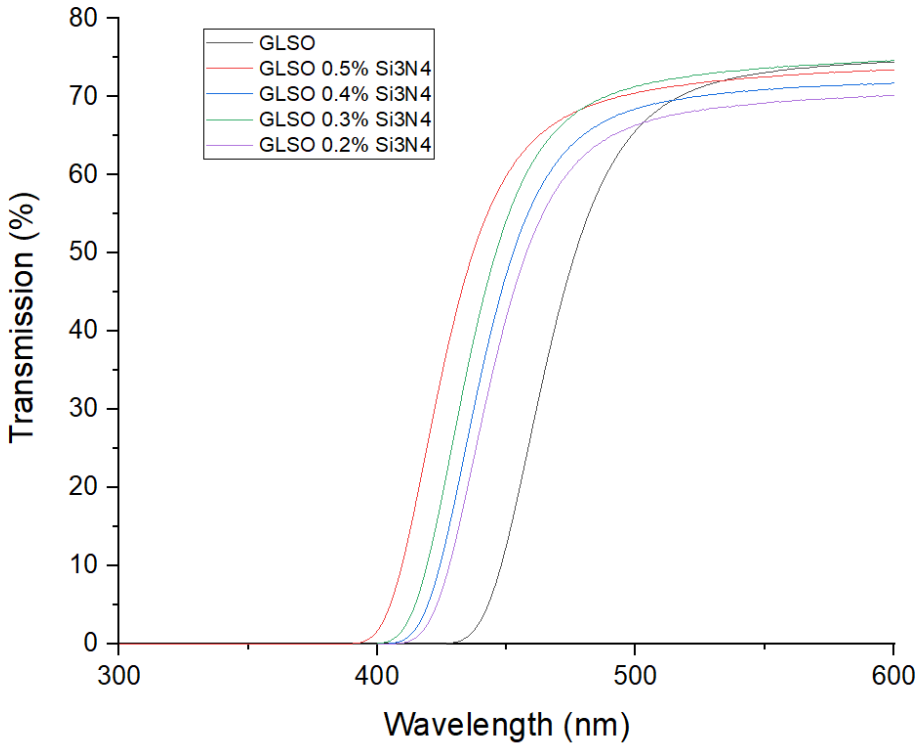

Figure 3. UV-Vis Spectra (0.2-1.66 um), zoomed in on visible cutoff region, of doped and undoped GLSO glasses.

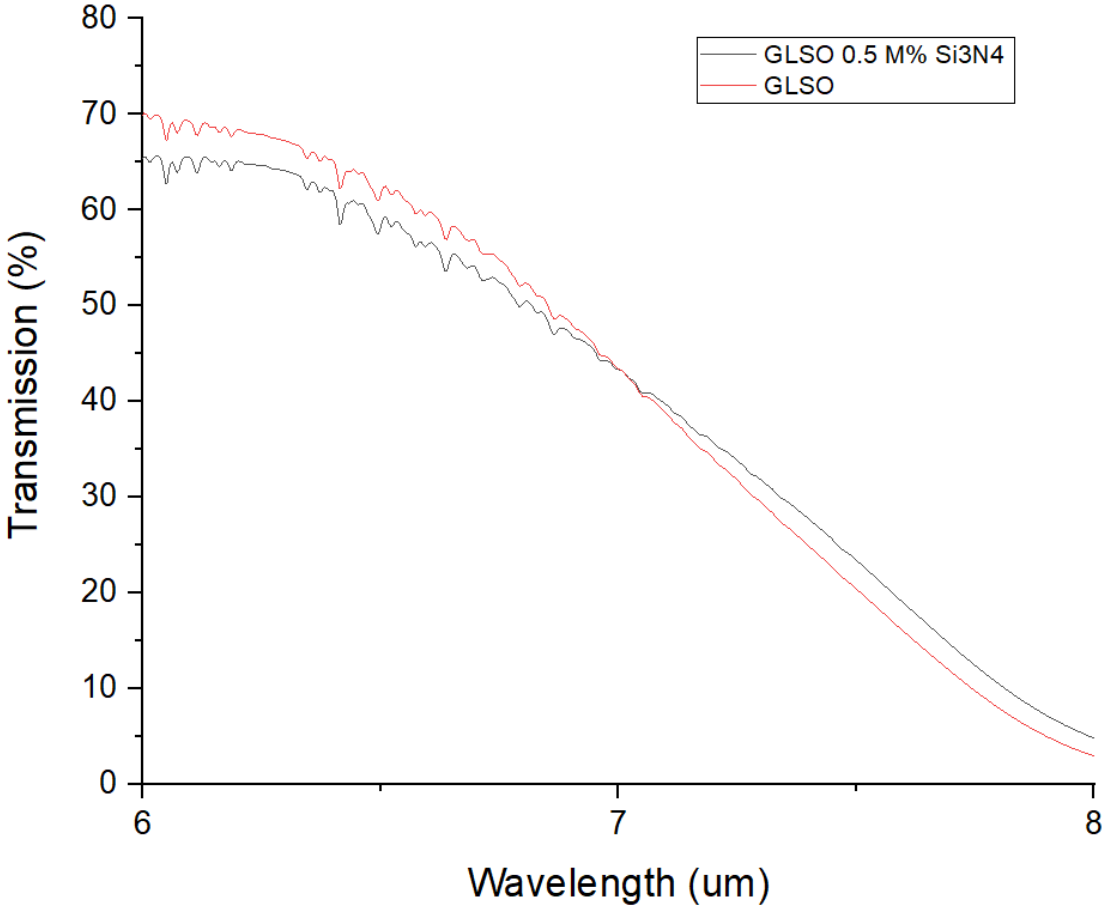

Figure 4. FTIR spectra (1.66-25 um), zoomed in to IR cutoff region, of 0.5 M% doped and undoped GLSO glass.

3.3 Mechanical Properties

To assess whether the hardness or reduced modulus of the material had been altered, nanoindentation was used with a variety of penetration depths. In general, the near-surface mechanical properties of a material have a high error and can fluctuate quite wildly. As the penetration depth becomes deeper, it begins to settle on the true bulk properties of the material. This is demonstrated quite clearly in the depth profiles of the undoped GLSO and the GLSO with the highest dopant (0.5 M%) (figures 5 & 6). Once at penetration depths over 500 nm, the measured results of both materials have smaller errors bars and settle on a bulk hardness and modulus. The results show slight increases in the hardness and reduced modulus for the doped glass when compared with the undoped glass. This is an excellent result considering the dopant that caused the blue shift did not detrimentally affect the hardness of the material, which is an important parameter for aerospace applications.

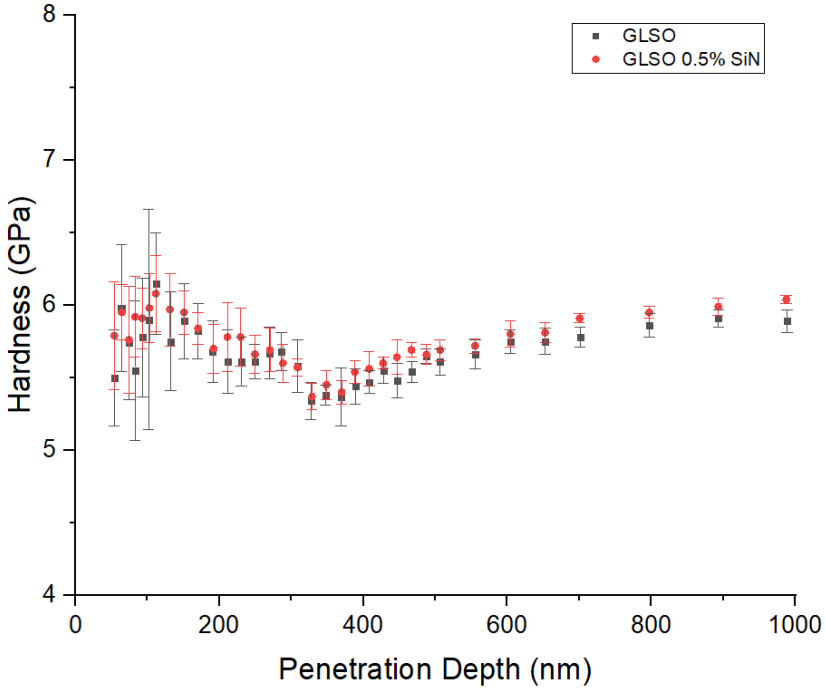

Figure 5. Hardness depth profile of doped and undoped GLSO from nanoindentation (50-1000 nm).

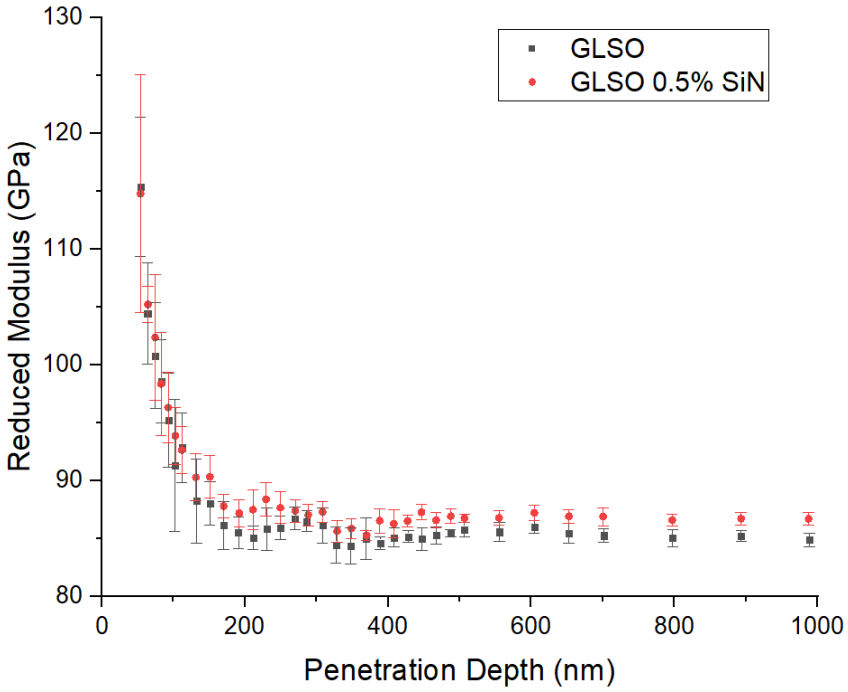

Figure 6. Reduced modulus depth profile of doped and undoped GLSO from nanoindentation (50-1000 nm).

4. CONCLUSIONS

The improvement in optical properties that the silicon nitride doping gave the GLSO, makes it an even more interesting material for visible-MWIR optics. Though other visible-MWIR materials, such as ALON, are mechanically and thermal robust, GLSO offers an alternative that is quicker, easier and safer to manufacture. Future work will be on using the dopants with the visible-LWIR GLS to see if similar results can be achieved, especially when combined with other dopants. Thermal analysis will be done on the doped samples also, to investigate any changes. Overall, this opens an interesting area of research, with low concentrations of nitrides yielding significant optical shifts.

REFERENCES

1. Livada, B. G. & Peric, D. EO/IR imaging systems countermeasures and camouflage: capabilities and new technological challenges. in *Proceedings Volume 11536, Target and Background Signatures VI; 115360D (2020)* https://doi.org/10.1117/12.2573469 vol. 11536 88–100 (SPIE, 2020).
2. Zeller, J. W. *et al.* Development of nanostructured antireflection coatings for infrared technologies and applications. in *Proceedings Volume 10404, Infrared Sensors, Devices, and Applications VII; 104040S (SPIE 2017)* 33 (SPIE-Intl Soc Optical Eng, 2017).
3. Göktug Genchan Artan & Galip Serdar Tombul. The future trends of EO/IR systems for ISR platforms. in *Image Sensing Technologies: Materials, Devices, Systems, and Applications* vol. 12091 76–88 (SPIE, 2022).
4. Telling, R. H., Jilbert, G. H. & Field, J. E. Erosion of aerospace materials by solid-particle impact. in *Window and Dome Technologies and Materials V* (ed. Tustison, R. W.) vol. 3060 56–67 (SPIE Proceedings, 1997).
5. Coad, E. J. & Field, J. E. Liquid impact resistance of CVD diamond and other infrared materials. in *Window and Dome Technologies and Materials V* vol. 3060 169–180 (SPIE Proceedings, 1997).
6. Sudha, P. N., Sangeetha, K., Jisha Kumari, A. V., Vanisri, N. & Rani, K. Corrosion of ceramic materials. in *Fundamental Biomaterials: Ceramics* 223–250 (Elsevier Inc., 2018).
7. Klein, C. A. Infrared missile domes: is there a figure of merit for thermal shock? in *Window and Dome Technologies and Materials III* (ed. Klocek, P.) vol. 1760 338–357 (SPIE, 1992).
8. Joseph, R. I., Tropf, W. J. & Thomas, M. E. Infrared transmission properties of sapphire, spinel, yttria, and ALON as a function of temperature and frequency. *Applied Optics, Vol. 27, Issue 2, pp. 239-245* **27**, 239–245 (1988).
9. Van Der Zwaag, S. & Field, J. E. Liquid jet impact damage on zinc sulphide. *J Mater Sci* **17**, 2625–2636 (1982).
10. Lucas, J. *et al.* Glasses to see beyond visible. *Comptes Rendus Chimie* **21**, 916–922 (2018).
11. Ravagli, A., Craig, C., Lincoln, J. & Hewak, D. W. Ga-La-S-Se glass for visible and thermal imaging. *Advanced Optical Technologies* **6**, 131–136 (2017).
12. Ledemi, Y. *et al.* Totally visible transparent chloro - Sulphide glasses based on Ga 2S3 - GeS2 - CsCl. *Journal of Optoelectronics and Advanced Materials* **9**, 3751–3755 (2007).
13. Masselin, P. *et al.* CsCl effect on the optical properties of the 80GeS 2-20Ga 2S 3 base glass. *Appl Phys A Mater Sci Process* **106**, 697–702 (2012).
14. Chen, G. & Cheng, J. Role of Nitrogen in the Crystallization of Silicon Nitride-Doped Chalcogenide Glasses. *Journal of the American Ceramic Society* (2004) doi:10.1111/j.1151-2916.1999.tb02184.x.

15. Uddin, M. S., Kwan, C. & Li, J. MWIRGAN: Unsupervised Visible-to-MWIR Image Translation with Generative Adversarial Network. *Electronics 2023, Vol. 12, Page 1039* **12**, 1039 (2023).
16. Hewak, D. W. *et al.* Chalcogenide glasses for photonics device applications. in *Photonic Glasses and Glass-Ceramics.* (ed. Murugan, G. S.) 29–102 (Research Signpost, 2010).
17. Oliver, W. C. & Pharr, G. M. An improved technique for determining hardness and elastic modulus using load and displacement sensing indentation experiments. *J Mater Res* **7**, 1564–1583 (1992).